

Plasmonically enhanced hot electron based photovoltaic device

Fatih B. Atar,^{1,2,*} Enes Battal,^{1,2} Levent E. Aygun,^{1,2} Bihter Daglar,²
Mehmet Bayindir,^{2,3} and Ali K. Okyay^{1,2,4}

¹Department of Electrical and Electronics Engineering, Bilkent University, Ankara 06800, Turkey

²UNAM-Institute of Materials Science and Nanotechnology, Bilkent University, Ankara 06800, Turkey

³Department of Physics, Bilkent University, Ankara 06800, Turkey

⁴aokyay@stanfordalumni.org

*fbatar@ee.bilkent.edu.tr

Abstract: Hot electron photovoltaics is emerging as a candidate for low cost and ultra thin solar cells. Plasmonic means can be utilized to significantly boost device efficiency. We separately form the tunneling metal-insulator-metal (MIM) junction for electron collection and the plasmon exciting MIM structure on top of each other, which provides high flexibility in plasmonic design and tunneling MIM design separately. We demonstrate close to one order of magnitude enhancement in the short circuit current at the resonance wavelengths.

©2013 Optical Society of America

OCIS codes: (040.5350) Photovoltaic; (240.6680) Surface plasmons.

References and links

1. M. W. Knight, H. Sobhani, P. Nordlander, and N. J. Halas, "Photodetection with active optical antennas," *Science* **332**(6030), 702–704 (2011).
 2. T. P. White and K. R. Catchpole, "Plasmon-enhanced internal photoemission for photovoltaics: Theoretical efficiency limits," *Appl. Phys. Lett.* **101**(7), 073905 (2012).
 3. M. Bareiß, F. Ante, D. Kälblein, G. Jegert, C. Jirasek, G. Scarpa, B. Fabel, E. M. Nelson, G. Timp, U. Zschieschang, H. Klauk, W. Porod, and P. Lugli, "High-yield transfer printing of metal-insulator-metal nanodiodes," *ACS Nano* **6**(3), 2853–2859 (2012).
 4. F. Wang and N. A. Melosh, "Plasmonic energy collection through hot carrier extraction," *Nano Lett.* **11**(12), 5426–5430 (2011).
 5. F. Wang and N. A. Melosh, "Theoretical analysis of hot electron collection in metal-insulator-metal devices," *Proc. SPIE* **8111**, 81110O, 81110O-6 (2011).
 6. C. Scales and P. Berini, "Thin-film schottky barrier photodetector models," *IEEE J. Quantum Electron.* **46**(5), 633–643 (2010).
 7. W. G. Spitzer, C. R. Crowell, and M. M. Atalla, "Mean free path of photoexcited electrons in Au," *Phys. Rev. Lett.* **8**(2), 57–58 (1962).
 8. J. C. Fisher and I. Giaever, "Tunneling through thin insulating layers," *J. Appl. Phys.* **32**(2), 172–177 (1961).
 9. E. D. Palik, *Handbook of Optical Constants of Solids* (Academic, 1998), Vol. 3.
 10. T. J. Bright, J. I. Watjen, Z. M. Zhang, C. Muratore, and A. A. Voevodin, "Optical properties of HfO₂ thin films deposited by magnetron sputtering: From the visible to the far-infrared," *Thin Solid Films* **520**(22), 6793–6802 (2012).
 11. Y.-C. Chang, S.-M. Wang, H.-C. Chung, C.-B. Tseng, and S.-H. Chang, "Observation of absorption-dominated bonding dark plasmon mode from metal-insulator-metal nanodisk arrays fabricated by nanospherical-lens lithography," *ACS Nano* **6**(4), 3390–3396 (2012).
 12. C. Lumde, S. Toroghi, and P. G. Kik, "Post-fabrication voltage controlled resonance tuning of nanoscale plasmonic antennas," *ACS Nano* **6**(7), 6301–6307 (2012).
 13. S. Ayas, H. Güner, B. Türker, O. O. Ekiz, F. Dirisaglik, A. K. Okyay, and A. Dâna, "Raman enhancement on a broadband meta-surface," *ACS Nano* **6**(8), 6852–6861 (2012).
 14. J. Kimling, M. Maier, B. Okenve, V. Kotaidis, H. Ballot, and A. Plech, "Turkevich method for gold nanoparticle synthesis revisited," *J. Phys. Chem. B* **110**(32), 15700–15707 (2006).
 15. S. H. Lim, W. Mar, P. Matheu, D. Derkacs, and E. T. Yu, "Photocurrent spectroscopy of optical absorption enhancement in silicon photodiodes via scattering from surface plasmon polaritons in gold nanoparticles," *J. Appl. Phys.* **101**(10), 104309 (2007).
 16. C. Rockstuhl and F. Lederer, "Photon management by metallic nanodiscs in thin film solar cells," *Appl. Phys. Lett.* **94**(21), 213102 (2009).
-

1. Introduction

Hot electron based devices are attracting significant attention in photovoltaic (PV) and photodetection applications. A hot electron based device can be very low cost and easy to fabricate, yet it can absorb light over a wide spectrum. Using plasmonic means to reveal the full potential of hot electron based devices has gathered great interest in the recent years. Knight *et al.* used nanoantennas on a photodetection scheme to excite surface plasmons under infrared light, generating hot carriers which are then injected over a Schottky barrier into a single crystalline Silicon [1]. A theoretical analysis on Schottky barrier hot electron photovoltaic devices estimated a maximum efficiency limit of 8% under standard solar illumination. More than 20% efficiency can be achieved if the electron density of states in the absorber could be modified [2]. Bareiß *et al.* fabricated a large array of metal-insulator-metal (MIM) pillar diodes (diameter < 100 nm) and used a conductive atomic force microscope (AFM) tip for the electrical characterization of individual pillar, showing promise for future photovoltaic applications [3]. A recent proof-of-concept demonstration of hot electron based photovoltaics was reported by Wang *et al.*; surface plasmons were excited at an MIM junction using a prism in Kretschmann arrangement and they showed up to $21 \times$ enhancement in the short circuit current at a single wavelength compared to no plasmon excitation condition [4]. They also theoretically analyzed patterning one side of the MIM junction to excite surface plasmons [5]. In this work, we propose a novel MIMIM hot electron PV device architecture with separate MIM junctions for tunneling (i.e. electron collection) and plasmon excitation. Such an approach allows independent optimization of the plasmon excitation and hot electron collection junctions. We experimentally demonstrate that the efficiency of MIM hot electron PV devices can be greatly enhanced by surface plasmon excitation.

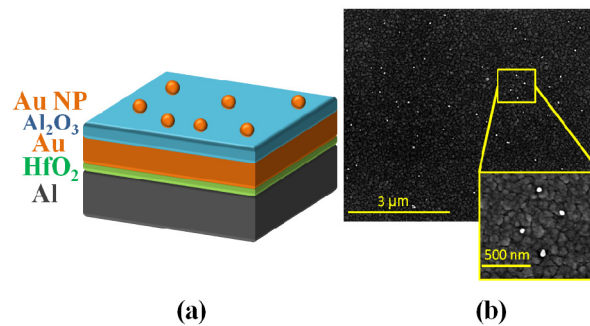


Fig. 1. (a) The schematic view of the hot electron based photovoltaic device. Au-HfO₂-Al layers form the tunneling junction, and Au NPs provide strong plasmonic field localization. (b) The top view SEM image of the completed device, showing the randomly distributed Au NPs with 50 nm diameter (bright white dots).

2. Theory

The first (bottom) MIM junction in the proposed device is formed by Au-HfO₂-Al layers. Then we complete the MIMIM structure by depositing gold nanoparticles on an insulating spacer layer (Al₂O₃) as depicted in Fig. 1(a). Au nanoparticle (NP)-Al₂O₃-Au layers and Au-HfO₂-Al layers constitute the top and bottom MIM junctions, respectively. Scanning electron microscope (SEM) image of the randomly distributed 50-nm-diameter nanoparticles on the device surface is shown in Fig. 1(b).

Energy band diagram of the bottom MIM (tunneling) junction in short circuit configuration is shown in Fig. 2. When an incident photon is absorbed, it can excite an electron in Au to a higher energy state and the excited hot electron starts diffusing in a random direction [6]. The distance that a photogenerated hot carrier can travel before losing its excess energy is limited by the mean free path of electrons in the metal (74 nm in Au) [7].

Therefore, hot carriers photogenerated in close proximity of the metal-insulator (Au-HfO₂) interface have much higher probability to reach the junction. A hot electron reaching the junction can tunnel through HfO₂ to Al and generate photocurrent (internal photoemission). An important parameter for device performance is the tunneling probability of hot electrons. The tunneling probability is strongly dependent on the insulator thickness [8] which was targeted 4 nm to obtain sufficiently high photocurrent. Lower insulator layer thicknesses could increase the tunneling rate (and improve efficiency), however we are constrained technologically in minimum thickness to form a continuous layer to avoid electrical shorting.

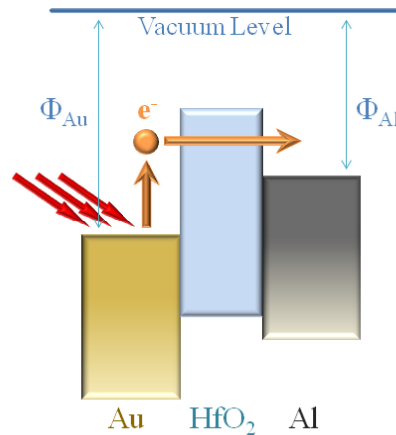


Fig. 2. The energy band diagram of the Au-HfO₂-Al MIM tunneling junction. The photoexcited hot electrons in Au diffuse towards the interface and tunnel through HfO₂ to Al, generating photocurrent (internal photoemission).

The hot carrier generation rate in the MIM device can be improved by enhancing the optical absorption in Au layer. Plasmonic structures can be incorporated to efficiently couple the incident light energy to the MIM device, increasing the optical absorption in Au. The incident photons can excite localized or propagating surface plasmons on the carefully designed metal surfaces and the surface plasmons can then decay, generating hot carriers [1]. Generated hot carriers can tunnel to Al to generate photocurrent (internal photoemission) or they can lose their energy in the form of heat. Local temperature increase due to surface plasmon absorption would also result in higher thermionic emission or tunneling rates through the junction. Our novel approach separates the plasmon excitation and hot electron collection (tunneling – rectification) mechanisms. Bottom MIM junction introduces the potential barrier and acts as a rectifying tunneling diode. Top MIM structure excites localized surface plasmons and resonantly couples the plasmonic energy to the bottom MIM structure.

A planar MIM structure is inherently a plasmonic waveguide which supports propagating surface plasmon modes at metal-insulator interfaces. However, these surface plasmon modes (dark modes) cannot be excited by normally incident light in a planar MIM configuration. However, scattering from an overlaying metallic nanoparticle could excite such waveguide modes. In order to investigate these effects, we performed simulations of the proposed structure with finite-difference time-domain analysis using FDTD Solutions by Lumerical Inc. We assumed a periodicity of 500 nm for the metal nanoparticles; high enough to prevent particle-to-particle interaction. Reported data from the literature is used for the dielectric constants of gold, aluminum, alumina and hafnia [9, 10]. We investigated the spectral absorption inside the flat gold metal layer with and without nanoparticles, illuminated with normally incident light. Resonant absorption enhancement occurs at about 590 nm. In Fig. 3(b), the electric field intensity profile of the plasmonically enhanced MIM structure is depicted at the resonant wavelength. NPs exhibit immense confinement of light into very

small volumes via localized surface plasmon (LSP) excitation. Excited LSP modes (due to NPs) interact with the underlying Au layer and trigger the dark modes in the top MIM [11]. Optical absorption at the top surface of the planar Au layer is significantly increased by this mechanism. The LSP modes also couple to the bottom MIM and excite propagating dark modes along the Au-HfO₂ interface. Resulting field localization increases the light absorption in the vicinity of the Au-HfO₂ junction, where photogenerated hot electrons have high probability of contributing to the photocurrent generation. Figure 3(a) shows the electric field intensity profile in a planar MIM structure without NPs ($\lambda = 590$ nm) for comparison. No surface plasmon mode is excited and only a very small fraction of the incident light could be absorbed in Au.

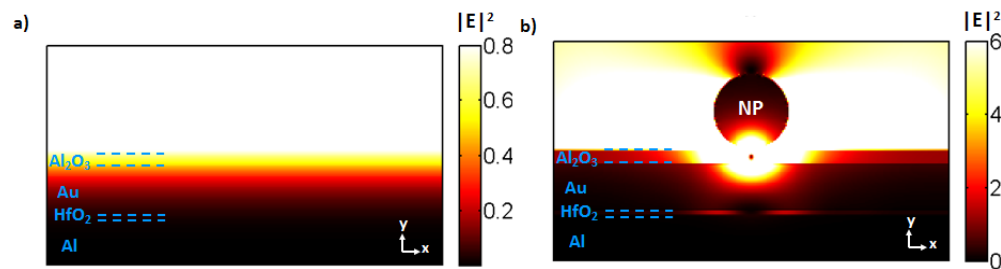


Fig. 3. Simulated electric field intensity profiles at wavelength $\lambda = 590$ nm. (a) Planar MIM structure without nanoparticles absorbs only a small fraction of the incoming light on the top portion of Au layer and most of the incident light is reflected from Au surface. (b) The incident light excites localized surface plasmons on Au nanoparticle which couple to the dark modes at metal-insulator interfaces.

In the proposed configuration, the center frequency, the strength and the width of the resonance can be controlled by the nanoparticle size, shape and distribution. The insulator thickness of the top MIM can also be tuned to control the resonance conditions [12, 13]. The thickness of the bottom insulator, however, is tightly constrained by the tunneling probability considerations.

3. Experiment

3.1 Fabrication

Though any substrate with sufficiently low surface roughness could be used, a Silicon wafer with ~ 300 -nm-thick SiO₂ was chosen as starting substrate. 150 nm Aluminum was thermally evaporated and patterned by photolithography and lift-off. 40-cycle HfO₂ was deposited in a Cambridge NanoTech Savannah atomic layer deposition system. A thin Cr layer was used as adhesion promoter followed by 30 nm Au evaporation. After patterning the Au layer, 150 nm Al was evaporated as the contact metal. 100-cycle Al₂O₃ was deposited as the top insulating layer.

Au NPs were synthesized by slightly modifying the Turkevich method. Sodium tris-citrate was used as the reducing agent at desired Au/citrate ratio to obtain NPs around 50 nm. Pre-heated citrate was added to the boiling gold solution under vigorous stirring [14]. Synthesized NPs were spin-coated on the Al₂O₃ layer in two steps to increase homogeneity, at 1000 rpm and 2000 rpm, respectively. Measured absorption spectrum of the synthesized Au NPs in de-ionized water solution is plotted in Fig. 4. NPs in solution show absorption resonance at around 530 nm wavelength.

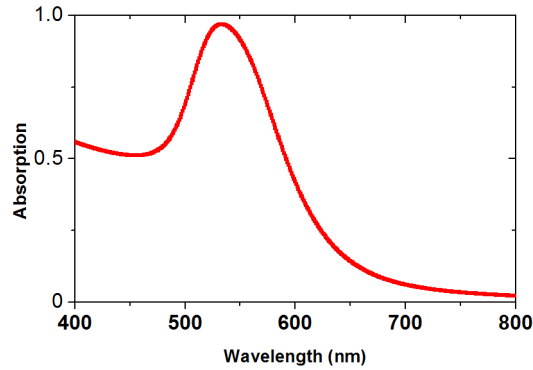


Fig. 4. Absorption spectrum of the synthesized Au nanoparticles in de-ionized water solution. NPs exhibit resonance at around 530 nm wavelength.

3.2 Measurement procedure

Device responsivity was characterized by short circuit current measurement under illumination. A Xenon-lamp illuminator and Oriel 74004 monochromator (1/8 meter, 1200 lines/mm grating) was used as light source in the 300-800 nm wavelength range. The monochromated light was collimated and mechanically chopped. The short circuit current was measured by a lock-in amplifier (SR830). A calibrated Si detector was used to record the spectral power from the light source. This was used to normalize the measured photocurrent to calculate the responsivity of the device at each wavelength. The illuminating beam size was larger than the active device area therefore the reported responsivity values here are slight underestimates.

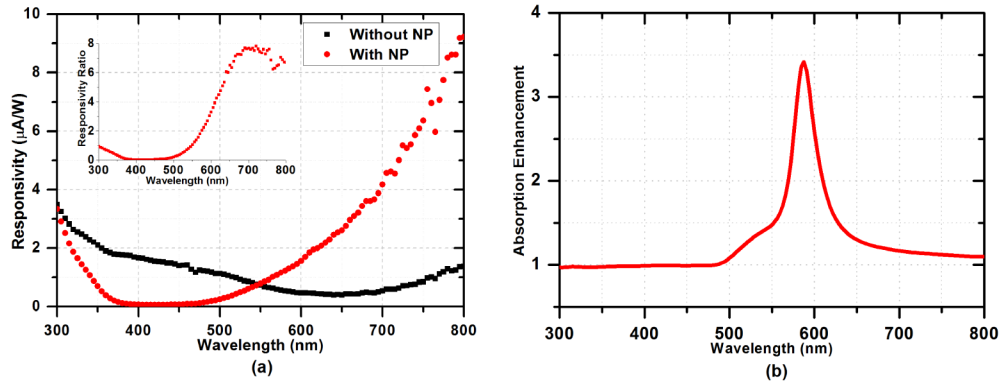


Fig. 5. (a) Measured responsivity of the device before and after nanoparticle spinning. The inset plots the responsivity ratio of the two measurements. The device with nanoparticles clearly shows resonant enhancement at 700 nm wavelength. (b) Absorption enhancement in the Au layer due to NPs, calculated with the FDTD simulation results.

3.3 Measurement results

Measured responsivity of a device before and after nanoparticle coating is plotted in Fig. 5(a). The plasmonic structure exhibits resonant photocurrent enhancement at around 700 nm wavelength. More than 7 times enhancement in the measured short circuit current with respect to the reference device is recorded at the resonance wavelength. Considering the relatively sparse distribution of the Au NPs [Fig. 1(b)], such an enhancement is quite significant and clearly shows that the efficiency of MIM photovoltaic devices can be greatly enhanced by surface plasmon excitation.

Enhanced absorption in the Au layer results in increased photocurrent. For comparison purposes, FDTD simulation results are used to calculate the absorption enhancement inside the Au layer due to NPs [Fig. 5(b)]. There is considerable similarity between the resonant behavior of the responsivity ratio [inset of Fig. 5(a)] and the computed absorption enhancement [Fig. 5(b)]. The experimental enhancement peak is red-shifted about 100 nm compared to simulation results. We attribute this shift to possible variation of dielectric properties of the experimental layers from literature values. In addition, surface roughness is neglected in the simulations that could affect the peak location.

Current-voltage measurements of the proposed device are performed under 1 sun solar simulator illumination. V_{OC} is measured to be 40 mV, and I_{SC} is 5 pA. Low photocurrent is attributed to thickness of insulator (HfO_2) layer in the bottom MIM junction. Insulator thickness and the junction quality can be further optimized to increase I_{SC} . The overall conversion efficiency is comparable to a recent proof-of-concept demonstration [4], where the measurements of the MIM device were done under focused helium-neon laser (633 nm) illumination in Kretschmann arrangement.

For our MIM configuration and NP size, the measured responsivity of the device drops below the noise level of the measurement system in the 400 nm - 500 nm wavelength range, which is not very accurately modeled in our simulation. A similar effect was observed by several groups for metal nanostructures on semiconductor absorbers [15, 16]. In such a structure two main electric field components arise: forward scattered field and directly transmitted field. At wavelengths shorter than the resonance wavelength of the metal nanoparticles, the phase difference between these two field components cause partially destructive interference, resulting in a decrease in the photocurrent [15, 16]. The portion of the incident light absorbed inside the NPs can also be considered to be lost since the hot carriers generated therein cannot contribute to the photocurrent due to the relatively thick (10 nm) insulation layer between the NP and the bottom MIM.

4. Conclusion

We demonstrate a new plasmonically enhanced hot electron based photovoltaic device where we separately form the hot electron collection and the plasmon excitation MIM junctions. We exploit resonant characteristics of Au nanoparticles to achieve high field localization in the MIM PV device. Au nanoparticles excite LSP modes and propagating surface plasmon modes, resulting in more than 7 fold enhancement in the short circuit current at the resonance wavelength. The simple planar MIM structure and use of chemically synthesized nanoparticles for plasmon excitation make this device promising for large area fabrication. We also show that plasmon excitation structures can be introduced without modifying the tunneling (rectifying) MIM junction. This gives additional degrees of freedom to optimize the electrical and optical properties of the MIM hot electron PV device. Different resonant structures, e.g. anti-reflection coatings, photonic crystals and cavities, and plasmonic structures, can be incorporated on any planar rectifying MIM junction with desired asymmetry and tunneling properties. Further studies can reveal a path for very low cost and sufficiently efficient photovoltaic cells.